AD-A116 015 CALIFORNIA UNIV BERKELEY DEPT OF PHYSIOLOGY-ANATOMY F/G 6/16
EFFECTS OF HIGH PRESSURE ON MEMBRANE ION BINDING AND TRANSPORT.(U)
DEC 80 R I MACEY, D M KARAN N00014-77-C-0482
UNCLASSIFIED NL

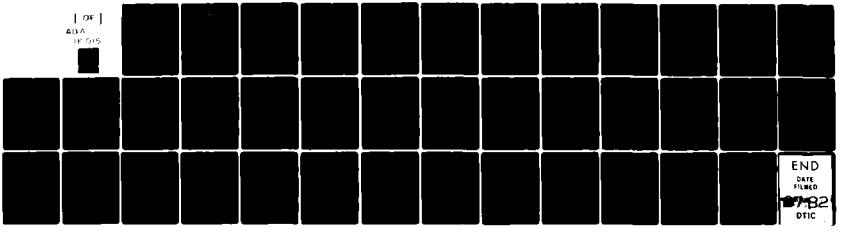

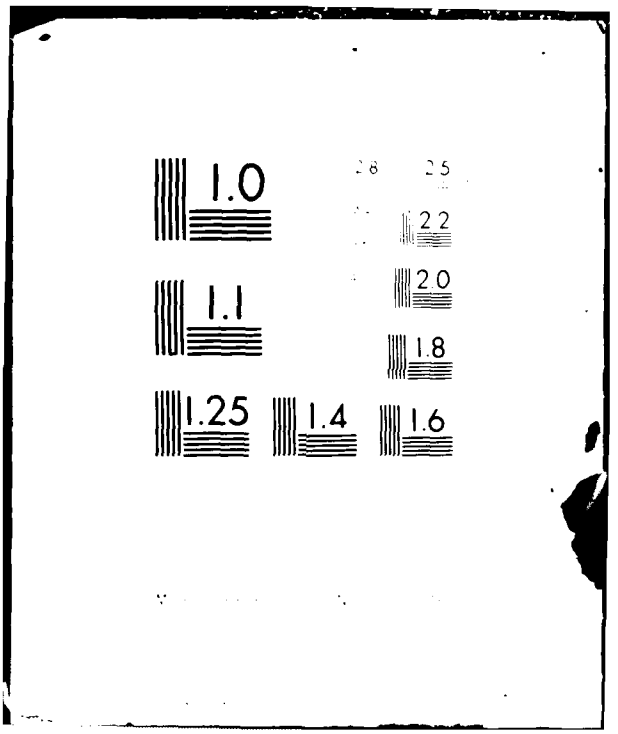
1.0
2.8
2.5
2.2
2.0
1.1
1.8
1.25
1.4
1.6

(1.2)

FINAL TECHNICAL REPORT

EFFECTS OF HIGH PRESSURE ON

MEMBRANE ION BINDING AND TRANSPORT
(N00014-77-C-0482)

Robert I. Macey, Ph.D.

and

Daniel M. Kiran, Ph.D.

Department of Physiology-Anatomy
University of California
Berkeley, CA 94720

This research was sponsored by the Office of Naval Research.

SECURITY CLASSIFICATION OF THIS PAGE (When Data Entered)

REPORT DOCUMENTATION PAGE	READ INSTRUCTIONS BEFORE COMPLETING FORM
1. REPORT NUMBER: Final Report	2. GOVT ACCESSION NO. AD-A116016	3. RECIPIENT'S CATALOG NUMBER
4. TITLE (and Subtitle): Effects of High Pressure on Membrane Ion Binding and Transport	5. TYPE OF REPORT & PERIOD COVERED: Final Report 6. PERFORMING ORG. REPORT NUMBER
7. AUTHOR(s): Robert I. Macey, Ph.D. Daniel M. Karan, Ph.D.	8. CONTRACT OR GRANT NUMBER(s): N00014-77-C-0482
9. PERFORMING ORGANIZATION NAME AND ADDRESS: The Regents of the Univ. of Calif. Univ. of California Berkeley, CA 94720	10. PROGRAM ELEMENT, PROJECT, TASK AREA & WORK UNIT NUMBERS
11. CONTROLLING OFFICE NAME AND ADDRESS: Office of Naval Research 800 N. Quincy St. Arlington, VA 22217	12. REPORT DATE: Dec. 31, 1980 13. NUMBER OF PAGES: 34
14. MONITORING AGENCY NAME & ADDRESS(if different from Controlling Office)	15. SECURITY CLASS (of this report): Unclassified 15a. DECLASSIFICATION/DOWNGRADING SCHEDULE

16. DISTRIBUTION STATEMENT (of this Report)
Unlimited reproduction in whole or part is permitted for any purpose of the United States Government

17. DISTRIBUTION STATEMENT (of the abstract entered in Block 20, if different from Report)
Unlimited

18. SUPPLEMENTARY NOTES

19. KEY WORDS (Continue on reverse side if necessary and identify by block number)
High pressure, red cells, permeability, water, calcium, potassium

20. ABSTRACT (Continue on reverse side if necessary and identify by block number)
Effects of hydrostatic pressures, ranging from 1 to 1000 atmospheres, on the transport and ion binding characteristics of human red cells were studied. A high pressure stopped-flow device was designed for rapid mixing and subsequent spectrophotometric study was designed and built with the following characteristics: operating pressures up to 1200 bar, minimum
(contd.)

DD FORM 1 JAN 73 1473 EDITION OF 1 NOV 65 IS OBSOLETE

Unclassified
SECURITY CLASSIFICATION OF THIS PAGE (When Data Entered)

Figure 6. Report Documentation Page.

average flow velocities equal to 2.0m/sec, dead time ranging from 5 to 25 msec.

Experimental results with red cells showed that 1) normal K^+ leakage increases dramatically at pressure > 6000 psi, 2) butanol induced K^+ leakage decreases dramatically at pressures > 6000 psi, 3) the Gardos response (K^+ leakage induced by A23187 + Ca^{++}) is reduced by pressure, and divalent cation selectivity sequences (Ca > Mg > Ba > Sr) do not change with 1000 atm pressure indicating that ionic radii are of predominant importance in binding, 4) loose Ca^{++} binding as measured by chlorotetracycline does not change with pressure, 5) both val+K^+ and butanol diffusion in red cell membranes have apparent activation volumes of 40 ml/mol in agreement with data on liposomes, and 6) perturbations in osmotic water flow through red cells by either high pressures or D_2O substitution can be predicted from the bulk properties of pure water.

TABLE OF CONTENTS

FIGURES

I. INTRODUCTION AND RATIONALE

Since high pressures influence any process which is accompanied by a change in volume, it can be expected to exert significant effects on reactions that are subject to changes in hydration and conformation. This is particularly true for electrolyte binding to and transfer through biological membranes. It is probably also true for non-electrolyte transport where carrier mediation and/or simple diffusion may be expected to require formation of "free volume" pockets within the membrane. High pressure perturbations are especially well-suited for the elucidation of these events because their effects can be attributed directly to changes in volume. Our long term objective is to investigate effects of hydrostatic pressure on the physiology of the human erythrocyte membrane in an effort to reveal fundamental mechanics of normal membrane structure and function. Accordingly, the results described in this report were obtained in "gas free" systems and are attributable to hydrostatic pressure alone.

We chose human red cells because they are the simplest and most abundant cell system available. They are devoid of internal organelles and membrane systems. They do not divide, synthesize protein or utilize oxygen. Their simple metabolism (almost limited to glycolysis) is sluggish and easily controlled. In contrast to giant cells (e.g., squid axons, algal cells), their plasma membrane is directly exposed to the extracellular medium. Finally, it is relatively easy to prepare isolated membranes and intact ghosts in quantity. Despite these intracellular simplifications, the red cell has a fully functioning cell membrane. It actively transports Na, K and Ca, and it has a facilitated diffusion system for glucose, amino acids, nucleotides, urea, HCO_3 and Cl. Red cell membranes respond to anesthetics in a manner similar to that of excitable membranes and are currently used as model systems in drug studies.

II. ELECTROLYTES/POLAR PATHWAYS

Ionic reactions characteristically involve hydration volume changes so that it is reasonable to expect a significant influence of pressure on electrolyte physiology. Accordingly, we have focused much of our attention on the ubiquitous role of metal ions in regulation of membrane processes. Interactions of cell membranes with Ca ions, for example, have been recognized as a requisite for nerve and muscle excitation, as a mediator in excitation-secretion coupling, as a trigger for muscle, ciliary and flagellar movements, and as an essential component in cellular adhesion and aggregation. Although the regulatory role of Ca in these events is established, the underlying physicochemical basis is not apparent.

With respect to the red cell, it possesses a powerful Ca pump and Ca activated actin and myosin-like proteins which play an important role in the maintenance of cell shape. Further, the K permeability of red cells is controlled by intracellular Ca and similar K channels (under similar control) have been identified in other cells. Finally, changes in Ca transport are implicated in red cell maturation, in sickle cell disease, and in microcytic spherocytosis.

A. Methods

Potassium fluxes were measured by suspending normal red cells in an isotonic buffered medium, containing either NaCl or NaCl + sucrose, and following changes in the K^+ content of medium. In some instances (NaCl medium) K^+ was measured directly with a K^+ electrode after the cells had been exposed to high pressures. In other instances (NaCl + sucrose), the K^+ content of the medium was estimated continuously during exposure to pressure through measurements of electrical conductivity. (In these cases the dominant electrolyte gradient favors KCl exit from the cell; as a result, changes in medium conductivity are almost entirely due to KCl efflux.)

B. Influence of Pressure on Potassium Permeability of the Normal Cell

Figure 1 shows a plot of K^+ flux vs pressure spanning a range of 1 to 1000 atm. obtained when normal cells are allowed to release their K contents into K free isotonic media. The results are plotted on a logarithmic scale, and are normalized to results at 1 atm. pressure. This facilitates computation of activation volumes and allows the results to be compared with similar measurements under different conditions. Figure 1 indicates that effects of pressure on normal K^+ flux increases dramatically with pressure in regions beyond 6000 psi. Although pressure also increases the free K^+ mobility in water, the sensitivity to pressure is much larger in the membrane than in water (this is also true for activation energies). Thus even if K^+ is moving through a simple water-filled channel, there must be considerable interaction with the membrane.

C. Influence of High Pressure on Butanol Induced Cation Leakage

Potassium leakage in the presence of 227 mM butanol as a function of pressure is shown in Figure 2. the data is normalized as in Figure 1, however, it should be noted that the absolute flux value obtained in this butanol treatment is an order of magnitude greater than the normal leak. The most striking feature is the very low pressure dependence below 6000 psi which increases precipitously beyond that point. Note that in contrast to normal K leakage, butanol induced leakage is inhibited by pressure.

In high concentrations of n-butanol, we expect the membrane to be exceptionally swollen with anesthetic, an apparent large $\Delta V^{\neq}$ above 8000 psi suggests that swelling is compensated at this pressure; the membrane is restored toward its original volume which is reflected by the decrease in cation leakage.

D. The Ca Induced K^+ Leakage (the Gardos Effect)

In order to initiate the Gardos Effect (Lew and Ferreira, 1977), Ca (or

FIGURE 1

Response of the Normal Cation Leak
In Human Red Cells to High Hydrostatic Pressure

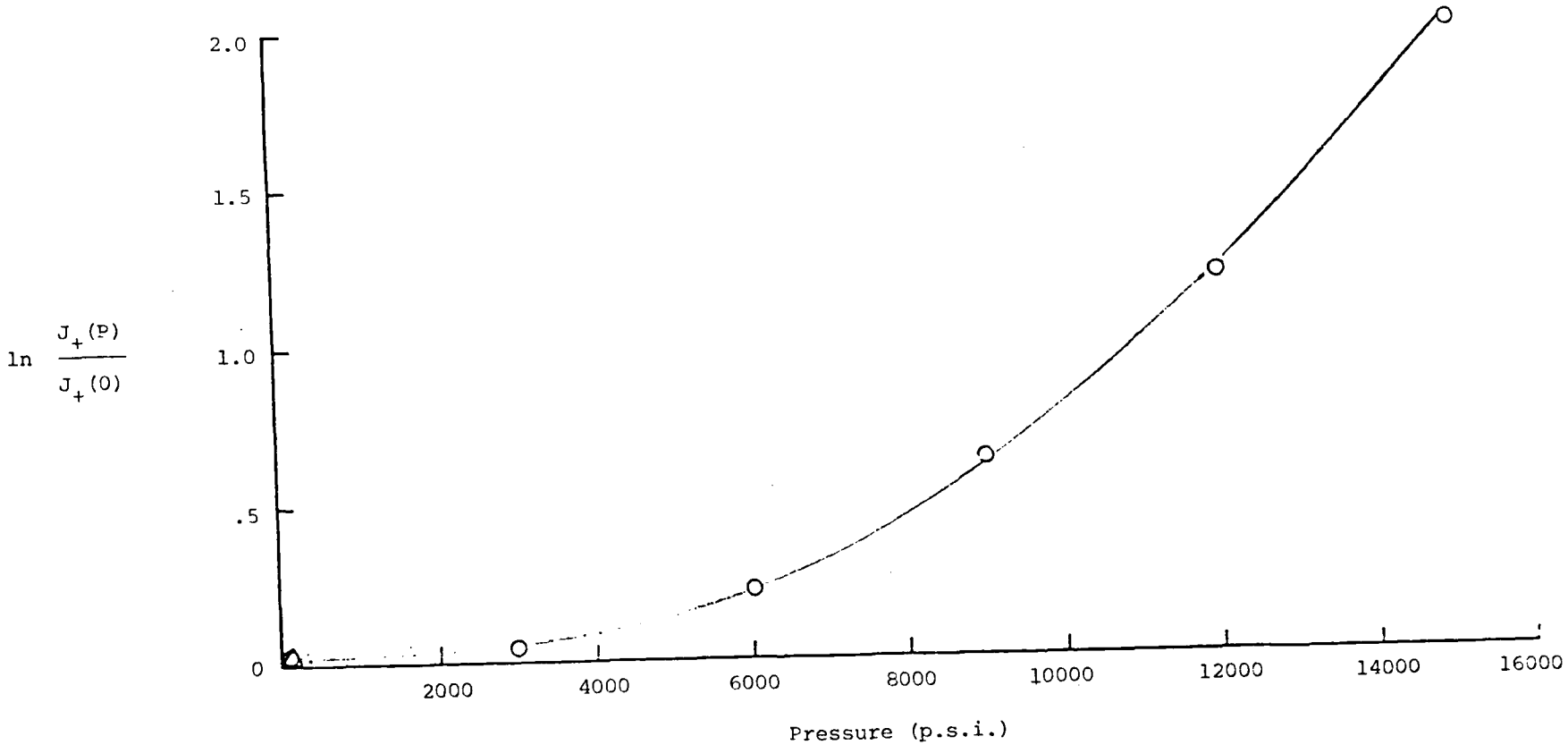

The vertical axis is the natural logarithm of the ratio of the net cationic efflux $J_+(P)$ at pressure P to the cationic efflux $J_+(0)$ at atmospheric pressure as measured by a change in external medium conductivity.

○ 15 mM NaCl and 270 mM sucrose

FIGURE 2

Response of the Anesthetic (n-Butanol) Induced) Cation Leak

In Human Red Cells to High Hydrostatic Pressure

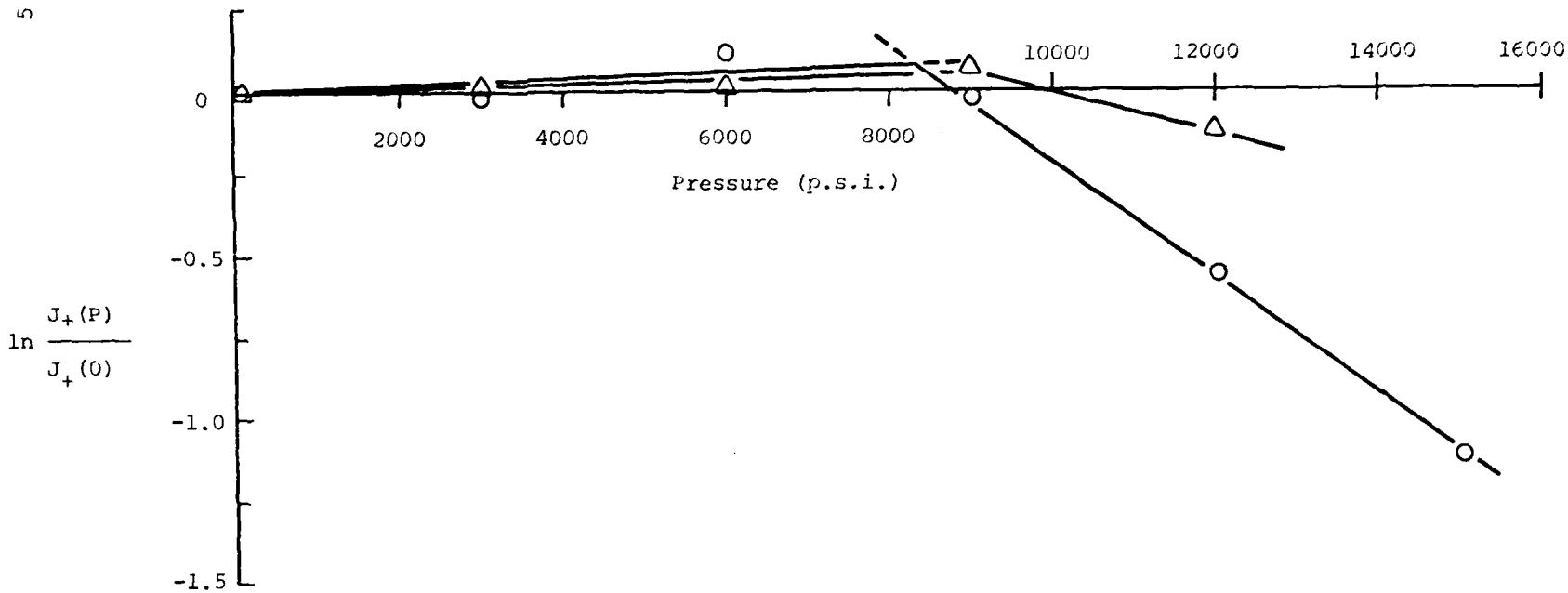

The vertical axis is the natural logarithm of the ratio of the net cationic efflux $J_+(P)$ at pressure P to the cationic efflux $J_+(0)$ at atmospheric pressure. 227 mM n-butanol is used to induce a substantial cation leak (Parpart and Green, 1951). The region around 8000 psi shows a marked transition in the pressure response.

---o——o— 15 mM NaCl and 270 mM sucrose

—Δ——Δ— 4.4 mM NaCl and 291 mM sucrose

some other divalent cation) must be introduced to the cell interior. This is commonly accomplished by using the Ca ionophore A-23187, and we have followed that procedure. This introduces minimal complication because the A-23187 mediated Ca transport process is very fast and because very small amounts of internal free Ca are required for a fully activated Gardos effect. Under these conditions, it is unlikely that Ca transport becomes rate limiting. The Gardos effect, then, begins with internal Ca reacting with some membrane receptor M and involves at least three steps:

1. Binding step: $Ca_{in} + M \longrightarrow CaM$

2. Gating step: K channel (closed) $\xrightarrow{Ca^{++}}$ K channel (open)

3. Transport step: $K^+_{in} \xrightarrow{\text{K channel (open)}} K^+_{out}$

Any, or all, of the above could contribute to the pressure dependence shown in Figure 3. However, data presented below suggests that the observed P dependence is not due to step 3, the transport of K^+.

Figure 4A presents data on the ability of a number of different divalent cations to substitute for Ca^{++} in producing the Gardos effect. Data is shown at two different pressures (1 and 1000 atm) and is arranged in order of increasing crystal ionic radii (decreasing hydrated radii). The most striking feature is that at 1 atm., the overall effect peaks at Ca^{++} and appears to fall off monotonically as the ionic radius is either increased or decreased beyond or below the radius for Ca. Clearly ionic radii play an important role in the overall Gardos effect at 1 atm. However, when pressure is applied, this simple dependence on ionic radius is no longer apparent. Data analysis is complicated by the fact that the Gardos effect is comprised of at least three processes (binding, gating, and transport). However, assuming that delivery of the cation

FIGURE 3

The Pressure Dependence of the
Calcium Induced Potassium Loss (Gardos Effect)

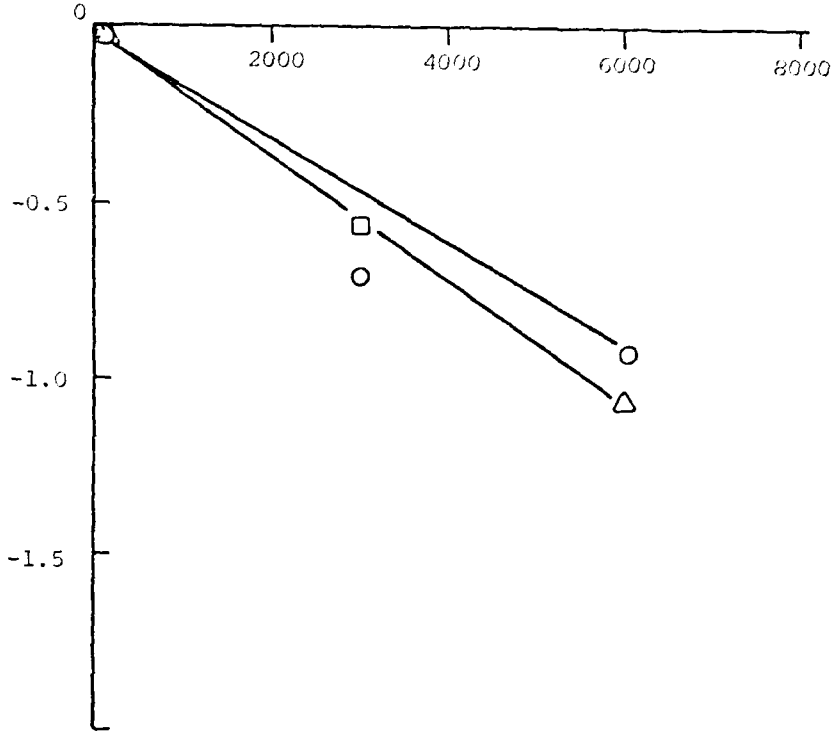

The curve shows the change in the natural logarithm of the ratio of the K^+ flux $J_K(P)$ at Pressure P to the K^+ flux $J_K(0)$ at atmospheric pressure for the calcium induced potassium leak in two different ionic strength media.

—o——o— 15 mM NaCl and 270 mM sucrose

—△ —△— 150 mM NaCl

LEGEND TO FIGURE 4

This bar graph shows the average K^+ flux in 10 minutes induced by 1 mM amounts of various divalent cations transported into the human red cell by the ionophore A23187. 15000 psi pressure was applied to 1/2 the sample after the flux was initiated, the remainder was used for an atmospheric pressure control.

Graph A shows the flux induced by each divalent cation alone (open bar) and its response to pressure (hatched bar). The divalent cations are arranged on the horizontal axis in order of increasing crystal ionic radii which is the order of decreasing hydrated radii. Graph B shows the flux induced by 1 mM Ca plus 1 mM each of seven other divalent cations. Hatch bars indicate the flux for each competitive system under 15000 psi pressure and open bars show the flux for each system at atmospheric pressure.

FIGURE 4

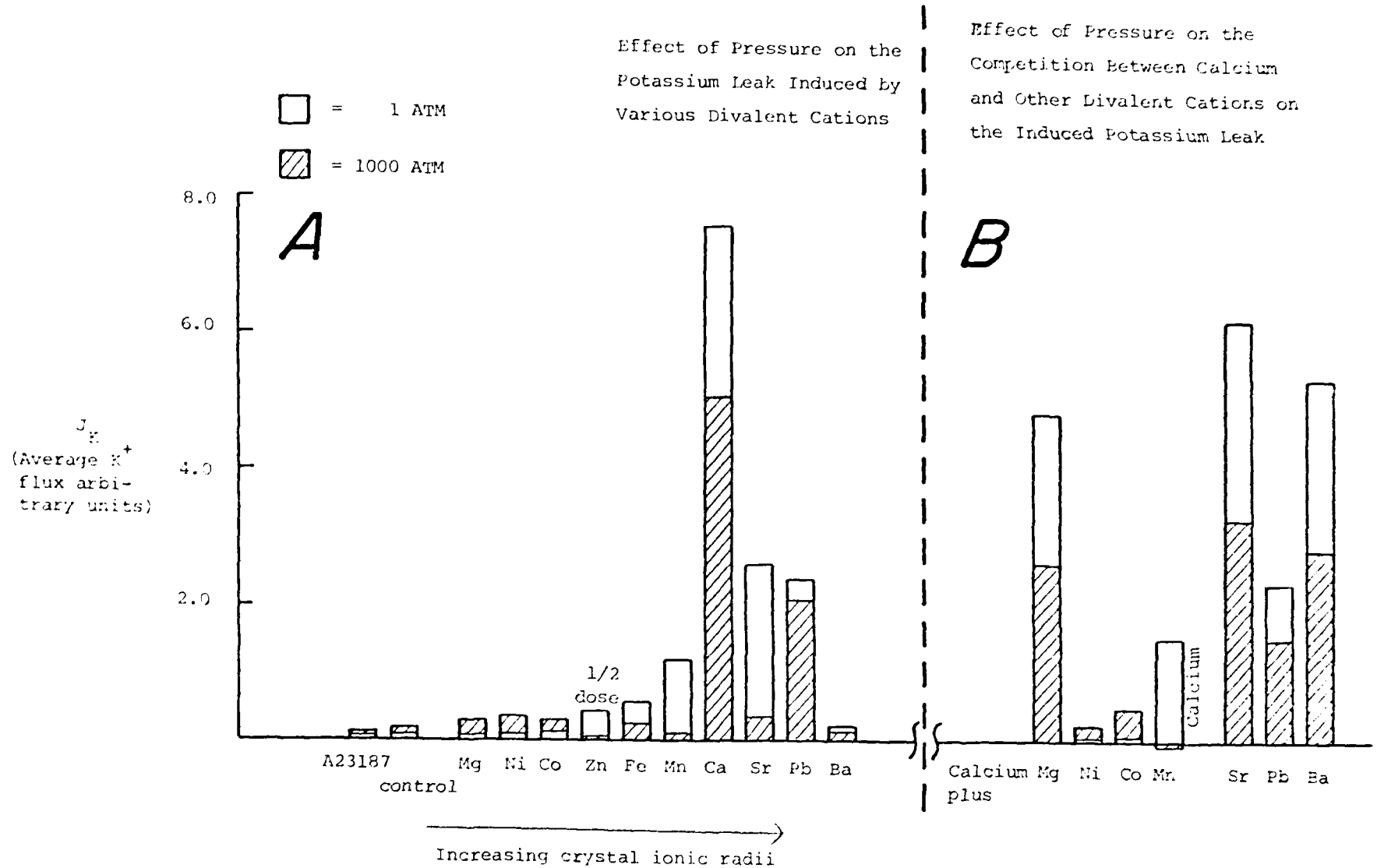
Effect of Pressure on the Potassium Leak Induced by Various Divalent Cations
Effect of Pressure on the Competition Between Calcium and Other Divalent Cations on the Induced Potassium Leak
= 1 ATM
= 1000 ATM
A
B
8.0
6.0
4.0
2.0
J_K (Average K^+ flux arbitrary units)
1/2 dose
Calcium
A23187 control
Mg Ni Co Zn Fe Mn Ca Sr Pb Ba
Calcium plus
Mg Ni Co Mn Sr Pb Ba
Increasing crystal ionic radii

by A23187 is rapid, we can eliminate transport from consideration as follows: If the effects of pressure on the Gardos effect result primarily from the transport step rather than binding or gating, we would expect the K^+ flux stimulated by each divalent cation to be reduced by a constant percentage when exposed to 1000 atm. Figure 4A shows this clearly not the case; if the data reflects the transport step at all, it must be in some combination with the other processes.

Competition studies shown in Figure 4B are more instructive because they refer to the binding site only. We restrict our attention to Ca, Mg, Ba, and Sr, because the possible selectivity sequences of these ions have been interpreted in terms of the electric field strength of the ion binding site together with considerations of hydrated and naked ionic radii (Diamond and Wright, 1969). In particular for these four cations, there are 4! = 24 possible permutations or sequences. Of these, only seven sequences (known as Eisenman sequences) occur naturally with any frequency.

Figure 4B shows that of the three ions, Mg^{2+} competes the most for Ca^{2+}, then Ba^{2+}, and finally Sr^{2+}, with Ca^{2+} being the most preferred of all. This sequence $Ca^{2+} > Mg^{2+} > Ba^{2+} > Sr^{2+}$ is Eisenman Sequence V. 15,000 psi does not alter this sequence. This indicates that probably in the intact membrane the binding sites do not move very much closer together. If they did, we would expect to find a shift toward Sequence VI which is not the case at all. At 1000 atm pressure, it is most likely that a fair amount of the structured water around the ions must be collapsed and yet this has no effect on the binding sequence (Podolsky, 1956; Drost-Hansen, 1972; Cuddeback et al, 1953). This indicates that the ionic radii are of predominant importance for the binding.

E. Loose Ca Binding

We have used the fluorescence of chlorotetracycline (Caswell, 1972;

Hallett et al., 1972) as a probe for the membrane (lipid) bound calcium. The pressure effect on the binding was studied over the pressure range 0-6000 psig in the fluorescence spectrophotometer in the specially constructed cuvette shown in Figure 5. Results illustrated in figure 6 show almost no change in the binding of Ca to the lipid protion of the membrane under 6000 psi. The loose binding constant calculates to be K_m = .2mM (which agrees with literature values -- c.f. Tolberg and Macey, 1972) for all pressures in the calcium concentration range .25-1.0mM.

The loose binding of calcium to the membrane has been attributed to the weak electric attraction provided by various contributions to the membrane surface charge. The main contribution comes from the lipid phosphate head groups (Schneider et al., 1978).

At 6000 psi, before th onset of any phase transition, we would not expect any change in field strength due to compression of the membrane. Johnson et al. (1973) found the compressibility of a phospholipid-cholesterol membrane to be 2.5×10^{-5} atm^{-1} which calculates to a change in linear distance of <.3% at 400 atm. The largest compressibility is found in n-dodecane (Cutter et al., 1953) which gives a linear change of 1.2% at 400 atm and 37°C. From this we would expect a change in field strength to be of the order of 1% at most in the PPC membrane.

Thus the results conform to expectations based on electrostatic field strength and compressibility. There is apparently no hydration change associated with this loose binding of calcium. A similar technique using terbium (Mikkelson and Wallach, 1974, 1976) could be used to study the high affinity sites which presumably would show stronger specificity and greater pressure sensitivity due to hydration reactions.

FIGURE 5

High Pressure Optical Cuvette

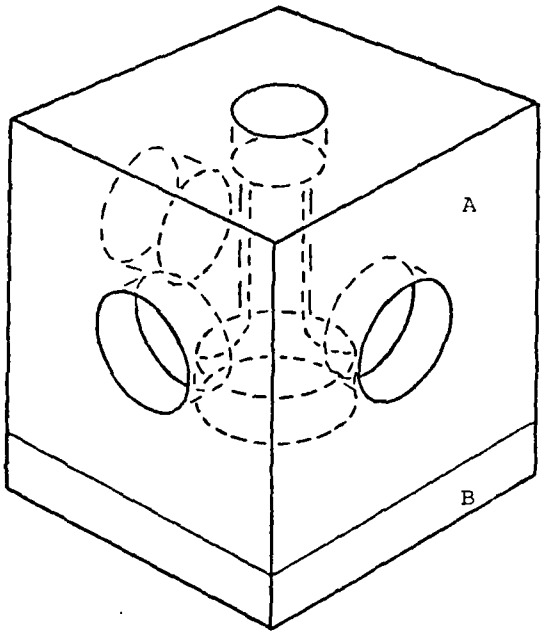

3-D View

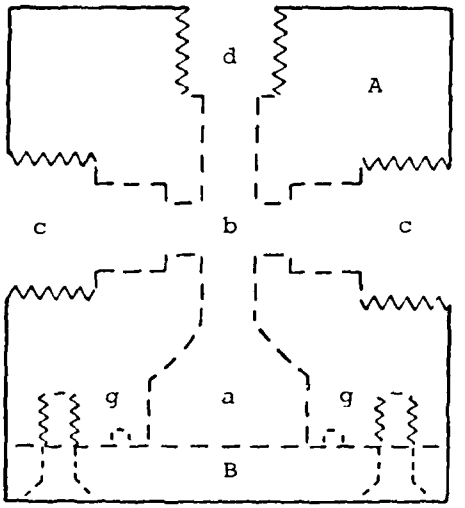

Cross-section

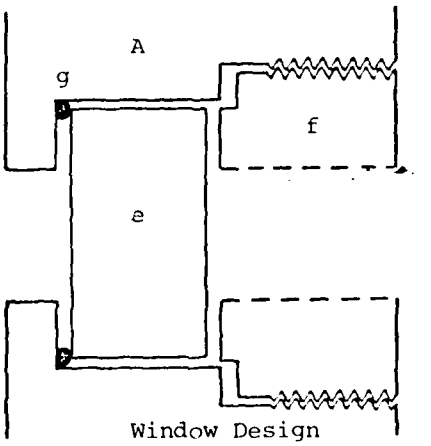

Window Design
Enlargement

A - body of high pressure cuvette (stainless steel)
B - bottom piece (stainless steel)
a - fluid cavity
b - observed fluid
c - observation window (3)
d - pressure entry port
e - quartz (or plastic) window
f - window retainer
g - o-rings

FIGURE 6

The Effect of Pressure on the

Loose Binding of Calcium

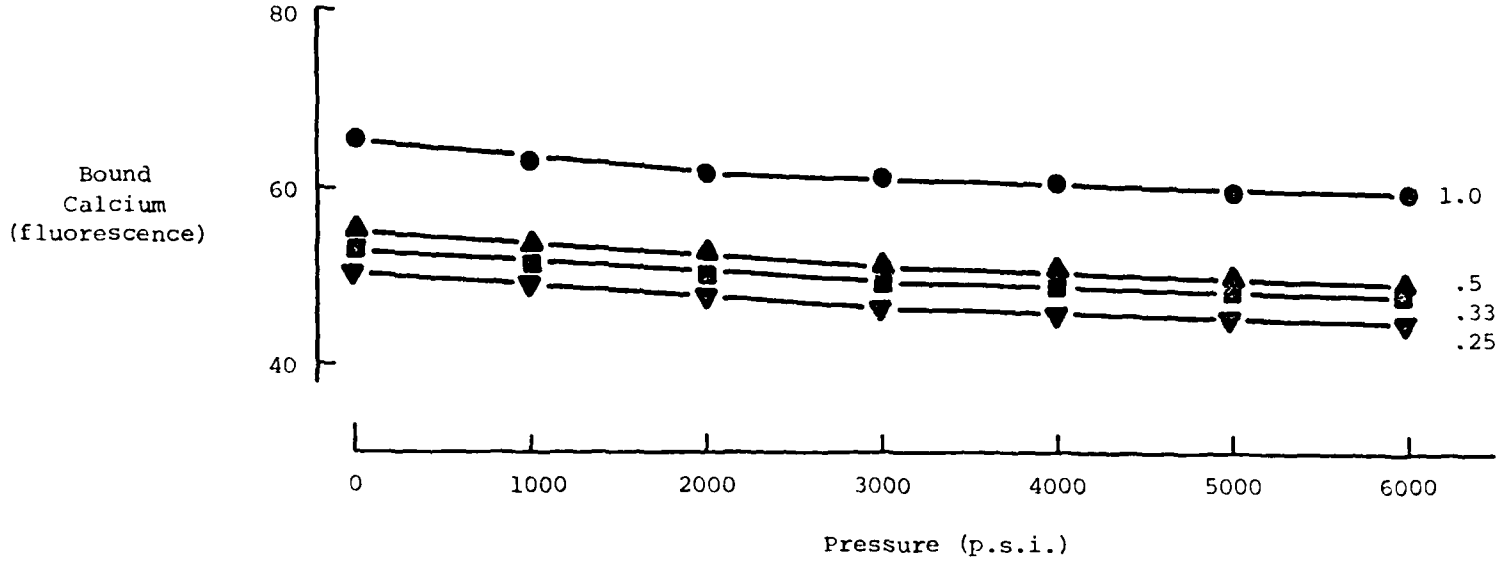

Effects of pressure on calcium binding to the red cell membrane as measured by chlorotetracycline fluorescence. The concentrations (mM) of free calcium in the medium are given next to each curve. The fluorescence scale is in arbitrary units. The loose binding constant $K_m \simeq .2$mM remains unchanged over the pressure range 0-6000 psig.

III. LIPID PATHWAYS

The ability of high hydrostatic pressure to displace exogenous lipid soluble substances from plasma membranes and thereby influence membrane transport is well known, particularly in the case of anesthetics. Our experiments with butanol induced K^+ permeability corroborate this. However, the use of high pressure as a fundamental tool for investigating lipid pathways goes beyond this.

Today there is universal acceptance that lipid solubility plays an essential role in permeation of cell membranes. However, there is continuing dispute over the role played by the size of the penetrating molecule, and how this is to be accounted for. Trauble (1971), for example, proposed that the migration of kinks down the acyl chain of fatty acids could account for diffusion of a solute through a lipid. The solute would fit into the space provided by the kink and migrate at the kink migration rate. Various type kinks are available so that solutes which were too large to fit into the volume provided by one kink could fit into the volume created by another type kink. The two smallest kinks considered are the 2g1 kink and the next largest, the 2g2 kink. In a quasi-solid system, Trauble estimates the 2g1 kink volume to 50-25$\AA^3$ which we calculate to be 30-15 ml/mole. In the fluid bilayers of red cells and liposomes, the value will be somewhat less. A 2g2 kink will have a larger volume than the 2g1 kink in any lipid system and will probably be approximately 2x volume of a 2g1 kink since the carbon is displaced one unit in the first and two units in the second.

Empirical measurements restricted to correlating permeability with molar volume have focused attention on the problem, of molecular size, but have yet to resolve the mechanism. Additional information is needed. Activation energies have provided some insights but they are of little use in the present context. Instead, mechanical information is needed that deals with the free volume of

the membrane and the changes it undergoes as it interacts with a permeating solution. Thus, it is natural to turn to pressure studies. For example, if the Träuble mechanism was responsible for transport through the lipid region of RBC's, we might expect to see the activation volume quantized around specific values for transport processes through the lipid pathway.

A. Can Results on Artificial Bilayers be Extrapolated to the Red Cell?

One of the simplest means of probing a lipid bilayer is to study its permeability to lipid soluble solutes such as the valinomycin-K^+ (val-K^+) complex. The question of similarity between red cell and artificial lipid membranes arises, for example, from the finding that the maximal val-K^+ permeability of the RBC is much lower than in artificial membranes. Is this due to a lowered absorption of val-K^+ into the membrane, or does it reflect a slower transport rate across the membrane?

We approached this problem by measuring the transport volume of val-K^+ in the red cell and comparing it with similar data from liposomes. Figure 7 shows a plot of our data taken over a range of 1 to 800 atm; the activation volume calculated from this data is 40 ml/mole.

Using liposomes, Johnson and Miller (1975) found that regardless of composition, the activation volume for val-K^+ transport was around 40 ml/mole in the range 0-400 atm. The reaction volume for complexation of K^+ with crown ethers (compounds similar to valinomycin) in water is around 8 to 12 ml (Isaacs, 1981). Thus, it seems unlikely that transport of val-K^+ is rate limited by reactions at the membrane interface. Since the val-K^+ complex is lipid soluble and traverses the lipid pathway in the RBC, the identical activation volume found in liposomes and red cells suggests of a similar if not identical transport mechanism, at least for val-K^+.

The Johnson Miller paper also reported an activation volume for both Na^+

FIGURE 7

Pressure Effect on the Valinomycin Induced
Potassium Loss in the Human Red Cell

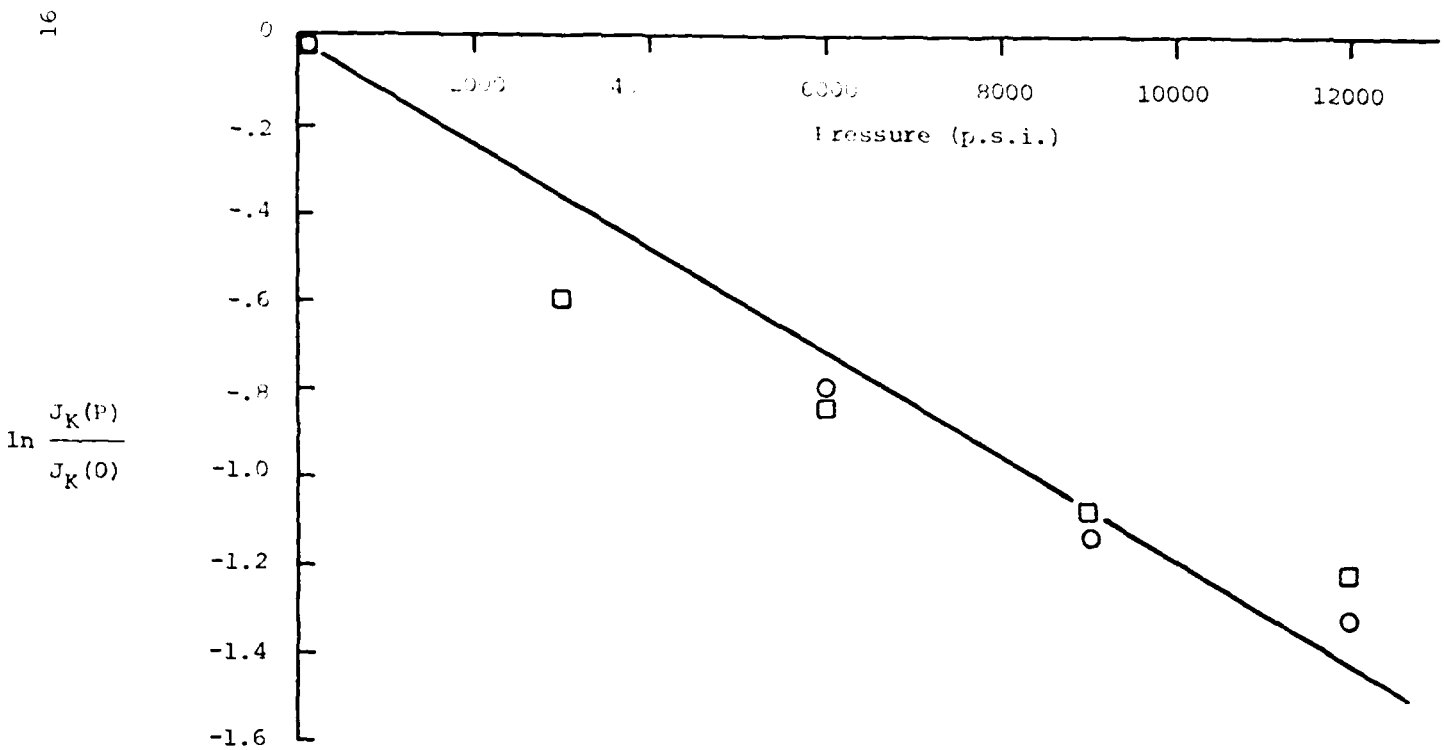

This graph shows the pressure inhibition of potassium-loss induced by 1μM valinomycin in human RBC's in 15 mM NaCl:270 mM sucrose, unbuffered. The activation volume 40 ml/mole given by the equation $\Delta V^{\neq} = -RT\ \Delta \ln (\frac{J(P)}{J(0)})/\Delta P$ is almost identical to that found for valinomycin induced potassium loss in liposomes of various compositions (Johnson and Miller, 1975).

and K^+ by themselves to be approximately 20 ml/mole. The liposome data can be interpreted in terms of the Träuble kink model (see above) which predicts that activation volumes would be multiples of some unitary volume -- say 20 ml. If the same transport mechanisms were operating in RBC's as in liposomes, we should find some lipid soluble substance whose activation volume would be 20 ml/mole in RBC's. Na^+ and K^+ are not suitable because their primary diffusion path is presumably associated with a protein portion of the membrane. However, the molecular n-Butanol which is lipid soluble was found to have an activation volume of 20 ml/mole (Figure 3) in RBC's for tracer diffusion through stacked membranes over the range 0-12000 psi.

This evidence suggests that the mechanism of transport through the lipid in RBC's is the same as transport in liposomes. Further, necessary evidence requires the correspondence of activation energies and volumes for the two systems for several lipid soluble solutes.

B. Pressure Dependence of Butanol Diffusion

In order to measure the pressure dependence of the permeability of a rapidly permeating solute, we have used two techniques. One involved the development of a high pressure stopped flow device which is described below. The other exploited the diffusion column technique introduced by DeWood et al., 1971. This latter method, a modification of a technique for diffusion measurements in agar gels developed by Schantz and Lauffer (1962), attempts to deduce permeability coefficients from bulk diffusion measurements through a "tissue" made up of packed erythrocytes. The erythrocytes are packed by centrifugation inside polyethylene tubing and the cell column is pulsed at one end with labeled solute. After diffusion has been proceeding for several hours, the distribution of label along the column is measured by sequential slicing and counting. The data is analyzed under the assumption of a diffusion model with intracellular

FIGURE 8

Pressure Effect on the Diffusion Coefficient

Of n-Butanol in Packed Human Red Cells

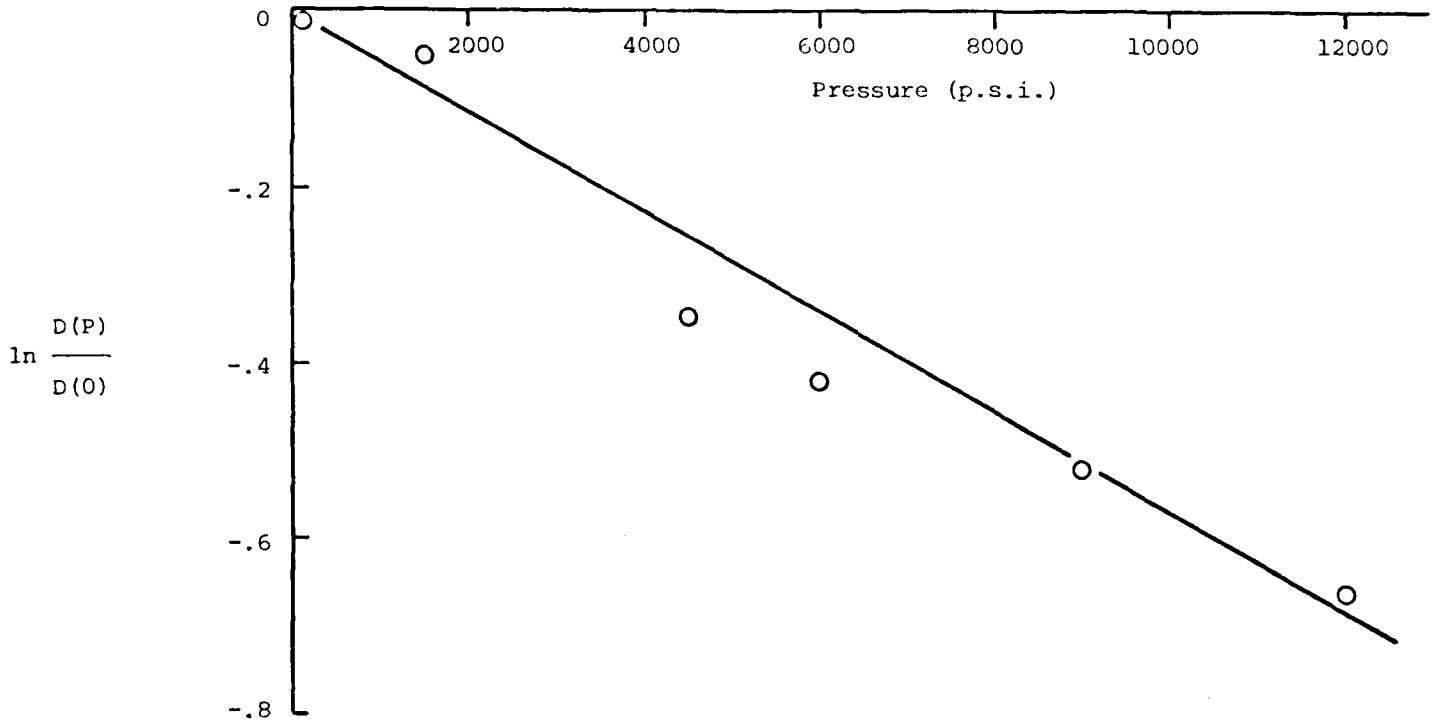

The diffusion coefficient measured here was obtained by modification of the method of Redwood et al (1974). The actual permeability of the cell membrane is related to the diffusion coefficient obtained in an algebraically complicated though almost linear manner. Therefore, the ratio of diffusion coefficients at pressure P to atmospheric pressure represents the ratio of cell membrane permeabilities.

The graph shows a change in the ln (ratio) for diffusion of n-butanol in packed RBC's in buffered KCl sucrose. The volume of activation is $\Delta V^{\neq} \simeq$ 20 ml/mole which is discussed in the text.

and extracellular pathways. With this method, the cells can be exposed to high pressures for several hours while diffusion is taking place over macroscopic distances. Perturbations of the established concentration profile are negligible during the few minutes required to depressurize the system and freeze the column.

Results of an experiment using this technique are illustrated in figure 8. The pressure dependence of butanol diffusion through stacked membranes appears to be described by an activation volume of about 20ml/mole.

Although there is insufficient data for reliable statistical estimates, it is interesting to note that the two probes (butanol and Val-K) for permeation through the red cell lipid bilayer give activation volumes that are multiples of 20ml/mole in accordance with the results on artificial lipid bilayers and the interpreatation given to TrÄuble's theory.

C. Development of a High Pressure Stop-Flow

Realization of the goals outlined in this project depends on the availability of precise methods that allow measurements over a large range of pressures. Unfortunately, conventional rapid mixing (e.g., by stop-flow) and sampling (e.g., centrifugation) techniques commonly used in cell physiology are not applicable to high pressure work in their current form. Accordingly, we have devoted a good deal of attention to the development of a high pressure stopped-flow apparatus.

This apparatus introduces two important advances in high pressure studies: 1) Two fluids can be rapidly mixed and stopped for observation under high pressure. The entire process can be accomplished within milliseconds and with no drop in pressure. 2) Many experiments can be performed repeatedly and reproducibly in a matter of minutes.

In our application, we photometrically monitor changes in red cell volume

produced by sudden changes in the red cell's external environment. These changes are produced by rapidly mixing a dilute blood cell suspension with another solution containing drugs and/or a variety of molecules. After mixing is achieved, the flow which passes through a specially constructed high pressure optical observation port, is stopped and measurements are taken.

The theory and techniques for obtaining a large amount of membrane parameter information from perturbation type measurements have been well worked out (Macey, 1978). Our innovation allows these measurements to be done over a large pressure range. The use of cell volume changes to measure permeability is not restricted to solutes that are transported via the lipid pathway; it is equally useful in measurements of polar solutes over either carrier mediated or channel paths, as in the case of water transport (see below).

With a simple adaptation, an observation port containing a conductivity probe is easily put in the mixed flow. In principle this would also work for other transducers. With no modifications at all, this apparatus can be used to study rapid enzyme kinetics by spectrophotometric methods. Details of the device are described in the following reprint.

High pressure stopped-flow apparatus for the rapid mixing and subsequent study of two fluids under high hydrostatic pressures

Daniel M. Karan and Robert I. Macey

Department of Physiology - Anatomy, University of California, Berkeley, California 94720

(Received 24 September 1979; accepted for publication 2 May 1980)

A stopped-flow apparatus is described for the rapid mixing and subsequent study of two dissimilar fluids under pressures up to 1200 bar. The device consists of two identical pressure chambers which contain the two fluids, a third pressure chamber which contains gas to maintain the pressure in the system, an optical port for photometric observation, and various connections. The device has been used to measure reaction times on the order of a hundred milliseconds to tens of seconds, using a maximum of 2 ml of each reagent per experimental determination. The dead time is found to be 5–25 ms with minium average flow velocities of 2.0 m/s. The construction and operation of the device are described and examples of water transport data in red blood cells and the bromophenolblue indicated chemical reaction of $NaHCO_3$ and HCl under pressure are presented.

PACS numbers: 07.35. + k, 82.40. − g, 07.60.Dq

INTRODUCTION

It was more than forty years ago that Roughton[1] first used a stopped-flow method for the rapid mixing of two separate fluids and the subsequent study of a reaction which was complete on the order of seconds. The method was perfected by B. Chance[2,3] a few years later for reaction times of a few milliseconds. Further advancement led to the Gibson–Durrum[4] and the Berger[5] apparatuses, with commercial development making stopped-flow equipment and techniques widely available.

Until the present, the only intensive thermodynamic parameter which could be varied in stopped-flow studies has been the temperature. The purpose of this paper is to describe a stopped-flow apparatus which we have built and are using in our laboratory for the photometric study of reactions at pressures up to 1200 bar. This new innovation allows the introduction of pressure as a thermodynamic variable in fast reactions requiring rapid mixing.

I. APPARATUS CONSTRUCTION

Figure 1 shows details of chamber A (1) of the high-pressure stopped-flow device illustrated in schematic form in Fig. 2. The body of chamber A (2) is made from 304 stainless steel machined to a smooth bore with inner diameter 3.88 cm, outer diameter 7.38 cm and 16.6 cm in length. The end caps (3) are machined from 304 stainless steel to fit the bore of the chamber with 0.08 mm maximum clearance. The pressure seal is provided by a Buna "O" ring (4). The entry into the end cap (5) is machined to take the standard 0.635 cm high pressure cone fitting. The cover (6), machined from 41-leaded-42 alloy steel, screws down over the body and holds the cap in place.

The interior of the chamber is separated into two compartments by a sliding piston (7) made of PVC plastic with a Buna "O" ring seal (8). (Note: the pistons have been modified to take two Buna "O" rings in place of the single "O" ring seal shown in Fig. 1.) The piston transfers the hydraulic pressure from the fluid in the lower chamber, which is in communication with the pump (22) and the gas-buffer chamber (14) (see Fig. 2), to the fluid in the upper chamber, which in the operation of the device itself is expelled under pressure. If the fluid is a suspension (e.g., red blood cells), a uniform distribution is maintained by means of a magnetic stir bar (9) surrounded by a PVC guard ring (10). The guard ring is essential to prevent the deformation of the piston around the magnetic stir bar when the piston reaches the upper end of its travel. The rotating magnetic field is provided by four electromagnets (11) with extended pole pieces (12)

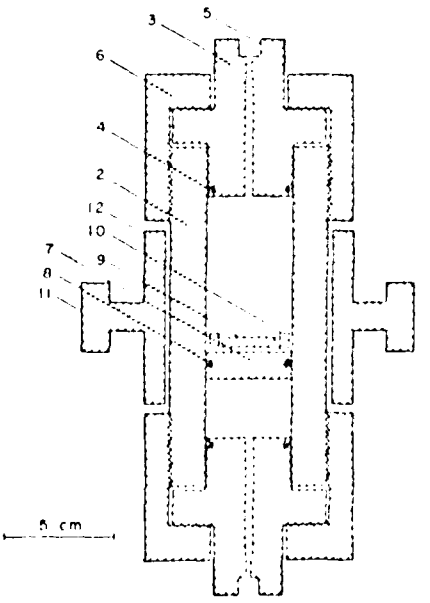

FIG. 1. Cross section of the stopped-flow high pressure chamber with the electromagnetic stirring device.

 0034-6748/80/081042-04$00.60

located 90° apart around the 304 stainless steel cylinder which is permeable to the magnetic field. The electromagnets are driven by a 12-V power supply with a switching circuit.

Figure 2 represents schematically the whole high pressure stopped-flow device. Chamber B (13) is an exact duplicate of chamber A (1) in construction, without the stirring equipment. The gas-buffer chamber (14) has the same construction as do chambers A and B, the only difference is the length of the cylindrical stainless steel body which is 29.2 cm. The upper part of the gas-buffer chamber (15) is filled with nitrogen gas through the valve (16) to a convenient starting pressure, with the piston (17) located at the lowest end of the chamber. The lower end of the chamber (18) is connected through a standard high pressure valve (19) by means of a high pressure tee (20) to the hydraulic pressure line (21) which is connected to the pump (22) and pressure gauge (23) through an isolation valve (24). The bottom end of both chambers A and B are connected by high pressure tees to the same hydraulic pressure line as the gas-buffer chamber. The upper compartments of chambers A and B, containing two dissimilar fluids, are connected by means of standard 0.635 cm stainless high pressure tubing (25) which meets in a high pressure tee (26) (High Pressure Equipment Co. #60-23 HF4) where mixing takes place. The reaction of the mixed fluids is monitored at the observation port (27) by means of a light source (28) and a photodetector (29). A three way valve (30) connects the observation port to an expansion chamber (31) whose volume regulates the total fluid flow per measurement. The expansion chamber is connected to a vacuum disposal by a valve (32) for removal of the spent fluid.

The observation port (27) is shown in detail in Fig. 3. The body (33) is made from a standard stainless steel cross (High Pressure Equipment Co.) which is milled to

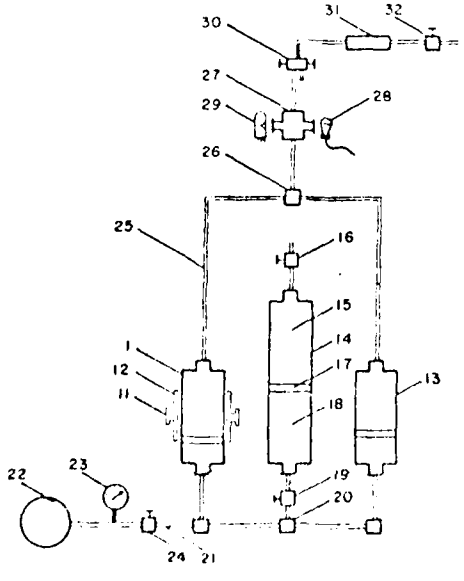

FIG. 2. Schematic view of the high-pressure stopped flow apparatus (see text).

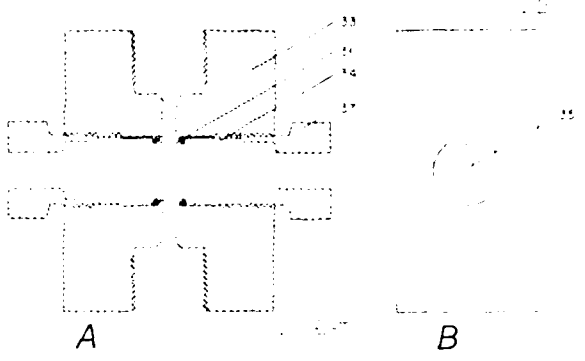

FIG. 3. (a) Cross section of the high pressure stopped-flow observation port. (b) Side view of observation port with window and gland nut removed.

within 0.5 mm of the central passage to allow the polycarbonate plastic optical windows (34) to be as close as possible to the fluid. A slot (35) is milled in the thin metal partitions on either side of the central passage to give the proper optical characteristics for measuring reactions in suspensions. A Buna "O" ring (36) supplies the pressure seal and a standard gland nut (37) which has been machined flat on the threaded end holds the window in place. Significantly higher pressure could be obtained by using synthetic sapphire windows,[5] though for our purposes polycarbonate plastic is adequate and inexpensive.

As a precautionary measure, the entire stopped-flow device was housed within a Lexan enclosure. Valves were operated by connecting rods extending out of the enclosure.

II. APPARATUS OPERATON AND TEST RESULTS

The high pressure stopped-flow operates in the following manner. A dilute blood suspension is placed in chamber A (1) where the electromagnetic stirrer keeps the suspension uniformally distributed. The test solution is placed in chamber B (13) and the two chambers are sealed to be pressurized. Valve (19) remains closed until the hydrostatic pressure matches the initial gas pressure in the gas-buffer chamber (14) at which time the valve (19) is opened. The gas and the fluid are then compressed together until achieving the pressure at which the measurement is to be taken. During the compression, the valves (30) and (32) remain closed and the expansion chamber (31) is empty of fluid.

The reaction is initiated by opening the pressure side of the three way valve (30). This allows the compressed gas (15) in the gas-buffer chamber to expand slightly, driving equal amounts of the two fluids from chambers A and B out through the mixing tee (26) and observation port (27), filling the expansion chamber (31). The fluid motion stops abruptly when the mixed fluids completely fill the expansion chamber at which time data gathering starts. The mixing rate is regulated by means of the valve (30); and the total volume flow for an experimental run is determined by the volume of the expansion chamber (31). When the measurement is complete, the pressure side of the valve (30) is closed. The valve (32) connected

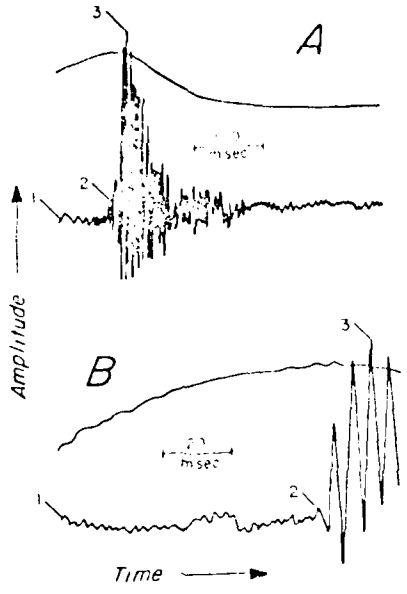

FIG. 4. Photometric time course of bromophenolblue indicated reaction between 0.02 M $NaHCO_3$ and 0.01 N HCl at 275 bar (smooth curves) with the simultaneous acoustic measurement of fluid flow (jagged curves). The upper set of traces (*A*) show the entire time course of the reaction while the lower set (*B*) show more detail of the first 100 ms. The initiation of flow (1), the beginning of deceleration (2) and full stop (3) are indicated (see text).

to a vacuum disposal and the atmospheric side of the three-way valve (30) are both opened, thus evacuating the expansion chamber. Then the valves are closed and the entire process can be repeated many times until the solutions in chambers A and B have been expended.

External temperature regulation is not necessary because the large mass of the system is very effective in maintaining a constant ambient temperature. (In our studies the variable of interest is pressure and although temperature is monitored, we have not attempted to systematically vary it.)

Figure 4 demonstrates the performance characteristics of the apparatus. The chemical reaction of 0.02 M $NaHCO_3$ and 0.01 N HCl with Bromophenolblue indicator at 275 bar is monitored photometrically (smooth traces) with the simultaneous acoustic measurement of fluid flow (jagged traces). (The flow duration was monitored acoustically by microphone because there are no external moving parts.) Figure 4(a) starts with the initiation of flow (1) then the beginning of deceleration (2) and full stop (3) while Fig. 4(b) expands the early part of the time course.

Although Fig. 4(b) shows almost no delay between full stop and the beginning of a measurable change due to the chemical reaction, we have sometimes found delays as long as 20 ms. (This delay time depends on operator skill in opening and closing the three way valve.) For the low flow velocity of 2.00 m s used in these measurements (for the sake of acoustics) and the 9.3 cm distance between mixing chamber and observation point, a minimum dead time of 4.6 ms is obtained. Though higher flow velocities are easily obtainable which would lower the transit time to the observation part, the dead time of the instrument should be conservatively taken to be from 5 to 25 ms.

Figure 5 shows an example of two photometric traces of the time course of human red cells shrinking in response to a sudden osmotic gradient obtained on this apparatus at 620 bar hydrostatic pressure. The upper trace is from cells treated with *p*-chloromercuriphenyl sulfonic acid (PCMBS), a sulfhydryl reagent which dramatically inhibits water transport.[7] The lower trace is from untreated cells. The large difference in the exponential decay time for cell shrinkage, i.e., $\tau = 0.41$ s (control) and $\tau = 4.61$ s (PCMBS) are well within the

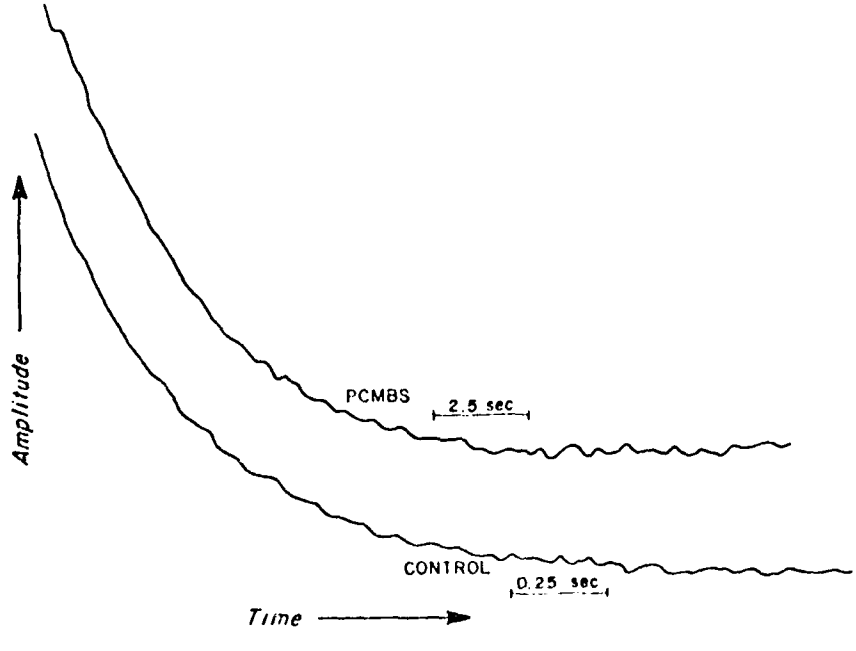

FIG. 5. Photometric trace of time course of red cell shrinking in response to a sudden osmotic gradient at 620 bar hydrostatic pressure. Upper trace: Cells treated with PCMBS. Lower trace: Control cells.

time span over which stable measurements can be taken. This indicates the wide range of reaction times which may be observed photometrically for various systems under pressure in the high pressure stopped-flow apparatus.

ACKNOWLEDGMENT

We wish to thank the Physiology-Anatomy shop personnel, in particular Ray Diaz for the machining of many of the components. Financial support by the Office of Naval Research, Contract #N00014-77-C-0482, NR201-188 is gratefully acknowledged.

[1] F. Roughton, Proc. Royal Soc. B **115**, 473 (1934).
[2] B. Chance, J. Franklin Inst. **229**, 455 (1940).
[3] B. Chance and V. Legallais, Rev. Sci. Instrum. **22**, 677 (1951).
[4] Q. H. Gibson and F. Milnes, Biochemistry J. **91**, 161 (1964).
[5] R. C. Bertert, B. Backo, W. Borcherdt, and W. Hauf, Rev. Sci. Instrum. **39**, 486 (1968).
[6] M. Yamada and V. H. Schmidt, Rev. Sci. Instrum. **49**, 1226 (1978).
[7] R. I. Macey, D. M. Karan, and R. F. J. Farmer, *Biomembranes*, edited by F. Kreuzer and J. Slegers. (Plenum, New York, 1972). Vol. 3, p. 331.

IV. WATER TRANSPORT

Results using the high pressure stopped-flow which show the pressure dependence of osmotic water permeability is illustrated in figure 9. The calculated activation volume is very small amounting to about 0.71 ml/mol. This is similar to the activation volume for water viscosity which ranges between 0.16 to 1.4ml/mol over the pressure range of 0 to 10kbar. The activation energy of osmotic permeability is also similar to activation energy of viscous flow, as are the perturbation effects introduced by mixing water the D_2O. Thus the properties of osmotic transport through red cells are predictable from the transport properties of pure water.

These results support the notion that osmotic flow in normal red cells takes place primarily through water-filled channels. The small activation volume does not support Träuble's original kink hypothesis for water transport in red cells. However, when the ostmotic channels are inhibited by PCMBS (parachloromercuribenzene sulfonate), preliminary results suggest that this is no longer the case; activation volumes become increasingly larger, reflecting the contribution of the lipid path.

Properties of D_2O transport through red cell membranes alluded to above are described in the following reprintt. They support the notion that the frictional forces encountered by bulk transport of water through channels are similar to corresponding forces in pure water.

JOURNAL OF CELLULAR PHYSIOLOGY 104:209-217 (1980)

The Permeability of the Human Red Cell to Deuterium Oxide (Heavy Water)

DANIEL M. KARAN AND ROBERT I. MACEY
Department of Physiology-Anatomy, University of California, Berkeley, California 94720

ABSTRACT Using a stopped-flow device, the osmotic water permeability of human red cells to D_2O and H_2O was studied as a function of temperature and under the influence of the sulfhydryl reagent parachloromercuribenzene sulfonic acid (PCMBS), an inhibitor of water transport. The ratio, permeability (D_2O)/permeability (H_2O) at each temperature can be predicted simply by assuming that permeability varies inversely with macroscopic viscosity. When water transport is inhibited with PCMBS, this dependency on viscosity vanishes; the inhibited permeabilities in D_2O and H_2O are indistinguishable.

The human red cell membrane has been a favorite prototype of studies of water transport for many years. Although experimental data are frequently interpreted in terms of water-filled channels ("pores"), progress in characterizing the channels has been slow because they are relatively insensitive to most transport reagents, and because it now appears that they are not traversed by any molecule, aside from water itself. Thus there is a paucity of channel "probes" that can be enlisted in the design of experiments. Given these circumstances, it would be expedient to exploit the small differences in physicochemical properties of D_2O and H_2O, both of which must have access to the water channels.

Rates of D_2O penetration into sheep, beef, and rat red cells have been measured by Brooks (35) and by Parpart (35). Both of these studies found a slower penetration by D_2O, and the results were interpreted in terms of differences in fugacities, viscosities and mobilities of the two solvents. However, these earlier investigators were handicapped by the scarcity of D_2O, the inaccurate physiochemical data available to them, and most important, by the fact that their measurements of water penetration were based on hemolysis times. In addition to water permeability, hemolysis times depend on a number of factors that are incidental to water transport; for example, these include prelytic electrolyte shifts and hemolytic volume.

There is no a priori reason to expect that any of these will remain constant when the aqueous environment is changed to D_2O. Accordingly we have restudied this problem with more modern techniques. We find that differences in the osmotic permeability of the human red cell to H_2O and D_2O can be quantitatively predicted solely in terms of differences in the macroscopic viscosity of these two solvents. Furthermore, when the channels are closed by saturating doses of mercurials, the difference in D_2O and H_2O permeability virtually disappears, and the apparent dependence of permeability on viscosity no longer holds.

METHODS

The equilibrium values for osmotic dead space b, and cell volume V were determined as follows: The plasma and buffy coat were removed from the red cells by centrifugation and vacuum aspiration and the cells were washed several additional times in isotonic KCl (π = 1.0 isotones). The final wash was in hypotonic KCl (π = 0.8), and the cells were resuspended to 38% hematocrit in the same solution. Ten milliliters of this suspension was pipetted into each of two small calibrated centrifuge tubes. These two tubes, each containing the same number of cells, were spun down and washed two times more. One tube was washed with π = 0.8(D_2O) (0.0895 gm KCl·10 ml D_2O); the other was washed with π = 0.8(H_2O) (0.0895 gm KCl·10 ml H_2O). After the last wash the cells were resuspended in π = 0.8(D_2O) and π = 0.8(H_2O) to the 10 ml mark. Hematocrits were taken of each sample, which gives the cell volume of one relative to the other.

Received February 13, 1980; accepted March 25, 1980

0021-9541/80/1042-0209$01.40

These samples were placed in a magnetically stirred, water jacketed beaker (T = 25° C) containing a conductivity probe. Small amounts of KCl crystals were added to the stirring suspension. The changes in salt concentration (or tonicity) was monitored by measuring the conductivity of the solution, and the resulting change in cell volume was measured by hematocrit. The process was repeated stepwise until the cells began to hemolize at high salt concentrations (π = 4). The value of b was determined by plotting volume versus $1/\pi$ for both H_2O and D_2O, where b is directly calculated from the extrapolated intercept at $1/\pi$ = 0.

The osmotic permeability coefficient RTL_p, for both D_2O and H_2O was estimated by monitoring the kinetics of cell volume changes after rapid mixing of cells (3% cells suspended in hypotonic, π = 0.9, solution) with an equal volume of hypertonic solution (π = 1.1) in a stopped-flow apparatus (Macey '79). All experiments were performed in KCl solutions or in KCl solutions with ½ the osmotic strength of the KCl replaced by sucrose to prevent unwanted swelling. Procedures for making D_2O or H_2O solutions were identical. Prior to usage, the cells were washed at least 3 times in KCl (or KCl + sucrose), the final packed pellet was resuspended in either KCl (D_2O) or KCl (H_2O). In some cases D_2O was reused, however in all cases the original D_2O was labeled with THO (.01 μCi/ml) in order to conveniently monitor any contamination of D_2O by H_2O. (Results showed that D_2O was never diluted by more than 2% H_2O per use.)

Stopped-flow mixing artifacts were minimized by subtracting control base lines (obtained by mixing isotonic cells with isotonic solutions) from the experimental data. Corrected data was then used to calculate osmotic permeability as described by Farmer and Macey ('70).

Temperature studies were run in a water jacketed stopped-flow where temperatures were monitored by a rapidly responding thermistor placed just beyond the light path where photometric measurements were made. Each temperature required an independent control baseline determination.

RESULTS

Figure 1 shows that the equilibrium osmotic properties of red cells are identical in H_2O and D_2O. At any given tonicity the measured cell volumes as well as the extrapolated osmotic dead space are indistinguishable in the two solvents. It follows that differences in rates of water equilibration in the two solvents can be attributed directly to differences in water permeability.

Table 1 summarizes our comparative data. Taking the average of 30 determinations at 25 C, the measured osmotic permeability in

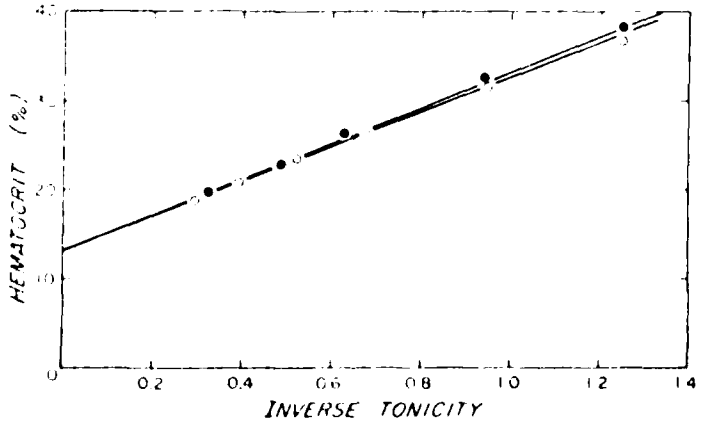

Fig. 1. Hematocrit versus inverse tonicity (normalized to unity at isotonic volume) as measured by ionic conductivity for human red cells in D_2O (open circles) and in H_2O (solid circles). The slope and the intercept for the two solvents are identical. The isotonic volume of the red cell is the same in D_2O and H_2O and the osmotic dead space b equals .40 in both D_2O and H_2O.

TABLE 1 Osmotic permeabilities of the red cell to H_2O and D_2O

Permeability to H_2O			Permeability to D_2O			
RTL_p ± S.E. (normalized)[1]	T° C.	Number of experimental runs	RTL_p ± S.E. (normalized)[1]	T° C.	Number of experimental runs	Donor
1.0 ± .01	25.0	30	.81 ± .01	25.0	34	A
.61 ± .02	10.4	12	.48 ± .02	10.2	16	B
.77 ± .01	16.5	14	.60 ± .02	14.2	8	
.63 ± .01	9.9	11	.51 ± .01	12.0	18	
.81 ± .01	16.2	14	.57 ± .01	16.7	16	C
1.0 ± .02	25.0	15	.88 ± .01	24.7	14	
1.38 ± .02	33.7	16	1.04 ± .02	33.1	13	
.59 ± .01	9.5	20	.45 ± .02	10.2	18	
.76 ± .01	16.1	14	.64 ± .01	16.2	26	D
.89 ± .02	23.6	16	.80 ± .02	24.0	12	
1.35 ± .03	32.2	15	.96 ± .02	32.8	20	

[1] All H_2O permeabilities are normalized to 1.0 at 25 C to correspond with the average value of RTL_p H_2O = 0.34 cm³ osM sec found from 30 experimental determinations at 25 C for donor A. The D_2O permeabilities are adjusted proportionately.

H_2O was 0.35 (± .004 S.E.) cm³ osM-sec. This compares favorably with previous determinations from this and other laboratories (Farmer and Macey, '70).

At 25 C, RTL_p is consistently about 20% lower in D_2O than in H_2O. This difference corresponds to viscosity differences of the two solvents; the result could be explained simply if RTL_p was inversely proportional to solvent viscosity; i.e., we assume

$$RTL_p(D_2O) = \frac{\eta(H_2O)}{\eta(D_2O)} RTL_p(H_2O) \quad (1)$$

where $\eta(H_2O)$ and $\eta(D_2O)$ are bulk viscosities of H_2O and D_2O, respectively. To test this, we took advantage of the dependence of viscosity on temperature as follows: First we determined the temperature dependence of RTL_p (H_2O) (data in Table 1) and found that, over the limited temperature range available to us, $RTL_p(H_2O)$ varied linearly with temperature. A least-squares fit of the data showed

$$RTL_p(H_2O) = .031\ T + .275 \quad (2)$$

If relation (2) is substituted into (1), together with empirical data relating $\eta(H_2O)$ and $\eta(D_2O)$ to T (Thomson, '63), then we obtain the predictions for $RTL_p(D_2O)$ as a function of temperature that are illustrated in *Figure 2*. Clearly all of our data can be predicted by this simple scaling procedure. This new function describing the osmotic response of the red cell in D_2O is predicted from the H_2O data solely by viscosity difference scaling. No other qualities of D_2O (i.e., reduced mobility, lower ionic conductance, etc.) are necessary to explain the lower permeability to D_2O.

The last result, shown in Figure 3, is the time course of PCMBS inhibition of water transport for D_2O and H_2O. The inhibition kinetics are slower in D_2O than in H_2O, perhaps due to isotope or solvent effects on the PCMBS + site binding reaction. Regardless of the binding kinetics, the permeability to D_2O in PCMBS treated cells appears to asymptomatically approach the limiting permeability found for H_2O in PCMBS treated cells. Since water is constrained to move through the lipid portion of PCMBS treated red cells (Macey et al., '72), two aspects of this transport become apparent from the asymptotic similarity in Figure 3: the permeability of the lipid portion of the red cell membrane is about the same for D_2O and H_2O, and the mechanism of transport through the lipid must be independent of the viscosity of D_2O and H_2O.

DISCUSSION

Thomson ('63) has outlined some of the ambiguities that arise when pH dependent rate processes are compared in D_2O and H_2O. These arise, at least in part, from the considerable difference in the D_2O and H_2O ionization constants. (For example, when pD = pH, pOD ≠ pOH). Fortunately, in our case these difficulties are minimized by the fact that the osmotic permeability of red cells is insensitive to pH (Rich et al., '68); the chief pH artifact in osmotic permeability determinations probably arises from pH dependent shifts in cell volume. Thus the chief criterion for adjusting pH (or pD) should ensure that cell volume is the same in both solvents. We have found (Fig. 1) that leaving the external medium unbuffered results in cell volumes and osmotic dead

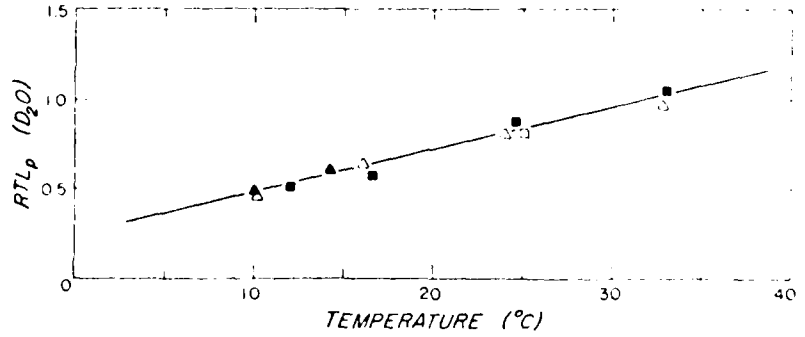

Fig. 2. Data points for $RTL_p(D_2O)$ at different temperatures taken from Table 1. Each characteristic symbol represents a different blood donor, and each point is the average of many experimental runs. The solid line is the theoretical prediction based on the $RTL_p(H_2O)$ data (See Results). All H_2O permeabilities are normalized to unity at 25°C.

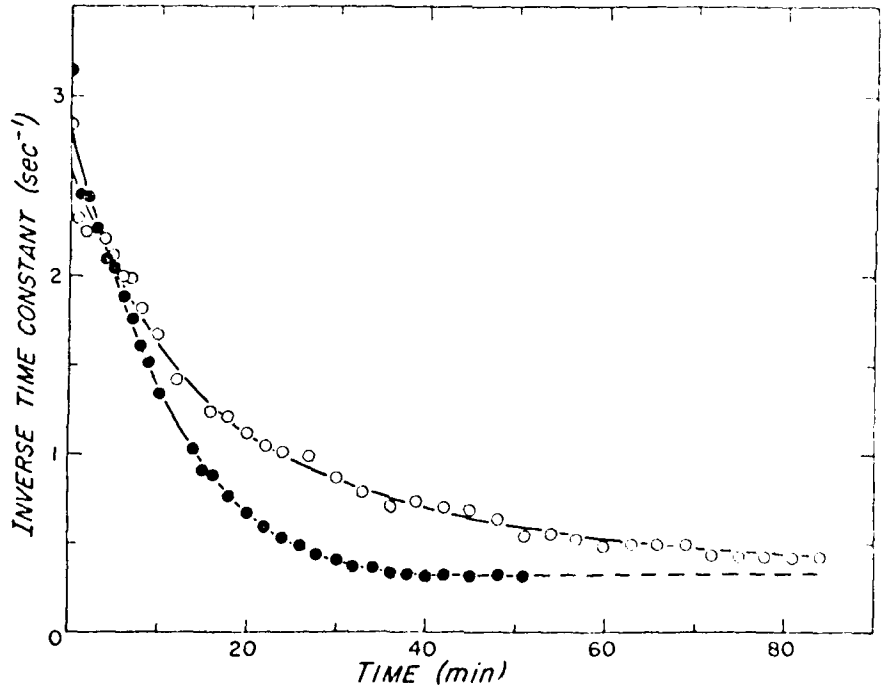

Fig. 3. PCMBS inhibition of D_2O (open circles) and H_2O (solid circles) transport as a function of time. The vertical axis is the inverse time constant (sec^{-1}), which is proportional to RTL_p. Each data point represents one experimental run. PCMBS concentration is 2 mM. The suspension and injection media have one-half the KCl replaced by sucrose to prevent cell swelling.

spaces that are identical in both D_2O and H_2O, and we have followed this practice. [This should not be misinterpreted to imply that the system is unbuffered. On the contrary, under these conditions, the enormous buffering capacity of hemoglobin will clamp the internal pH to a constant value (Macey et al., '78) and the presence of ambient CO_2 will ensure extra and intracellular H (or D) ion coupling through bicarbonate chloride exchange.]

Results reported by Owicki et al ('75) show essentially no difference in the cluster size, cluster distribution, or hydrogen bond energy between D_2O and H_2O in free solution. They found the two liquids to be structurally quite similar. Thus it is reasonable to find the cell volume and osmotic dead space are the same in the two solvents.

The earliest measurements of the red cell permeability to D_2O and H_2O were done by Parpart ('35) and Brooks ('35). Their estimates based on hemolysis times, ranged from a 22% to 44% decrease in permeability of the red cell for D_2O compared to H_2O. Even though the reported value for the viscosity of D_2O was greater in those days than more recently reported values, it still was not great enough to explain the large decrease in permeability to D_2O. Parpart suggested that D_2O's lower mobility (41% less than H_2O) could account for the discrepancy. We have found by modern techniques that the lower permeability of normal red cells to D_2O is due solely to the larger viscosity of D_2O.

The notion that osmotic flow through cell membranes should be inversely proportional to viscosity is not particularly new. It is explicit in the calculations of the equivalent pore radius (Solomon '68) and is demonstrated by experiments that show that the activation energies for L_p and bulk viscosity, η are of equal magnitude and opposite sign. This is seen in the product $L_p\eta$ independent of T (Viena et al., '70). The results of our paper lend additional support to this notion. However, this is not intended to imply that water flows through the red cell membrane in a continuum several layers thick. Experimental evidence is, in fact, to the contrary. The size of the calculated equivalent pore radius is too small to be consistent with the assumption of a gross continuum as well as the observed exclusion of small polar nonelectrolytes from the water channels (Farmer and Macey '70).

This problem of hydraulic flow in a narrow channel (3.2 Å radius) was studied in detail by Levitt ('73). Using statistical mechanical methods (Monte Carlo), he calculated the expected flow for a hard sphere dense gas model of water. He found that the formal application of Poiseuille's equation yielded the same results as his calculations, even though the molecular details of transport does not resemble bulk viscous flow.

It is also interesting to note that water restricted to the narrow channels of a gramicidin pore (2 Å radius) appears to be similar to bulk water. For example, in 99% D_2O the ionic conductivity through the gramicidin pore is decreased by about 20% (the same percentage decrease as seen for electrolyte conductivity in free solution) (Finkelstein '74). Thus the apparent dependence of permeability on viscosity has more than one explanation and does not necessarily imply laminar flow.

In PCMBS treated cells where water has been constrained to traverse the lipid pathway, viscous flow is no longer the mechanism of transport. This is simply seen from the 12 kcal mole activation energy for H_2O transport in PCMBS treated cells (Macey et al., '72). This high activation energy implies that almost all the hydrogen bonds are broken in the transport process through the lipid, which in turn suggests that water exists mostly as separate molecules inside the lipid moiety. The mechanism of transport through lipids would therefore treat H_2O and D_2O identically, since viscosity is no longer important and since the hydrogen bond energy is essentially identical.

In Figure 3, we see that the rate of transport for D_2O through the lipid portion of the red cell membrane asymptotically approaches from above the rate of transport for H_2O in the lipid portion of the membrane. Though the kinetics of inhibition are slower in D_2O, the final transport rate appears unaffected. Many models for transport through the lipid bilayer have been proposed that do not depend on the viscosity of water. Of these, the "kink" model proposed by Trauble ('71) is very attractive due to its simplicity. This model, where "kinks" (empty or full) migrate along the acyl chains in the lipid moiety, would transport D_2O and H_2O at the same rate in accordance with the results we found. We are doing further work, using high hydrostatic pressures, to evaluate the validity of the "kink" model of transport.

ACKNOWLEDGMENTS

This research was supported by the Office of Naval Research contract #N00014-77-C-0182, NR201-188 and NIH Grant #GM18849-07.

LITERATURE CITED

Brooks, S.C. (1935) The permeability of erythrocytes to deuterium oxide (heavy water). J. Cell. comp. Physiol., 7:163–171.

Farmer, R.E.L., and R.I. Macey (1970) Perturbation of *red cell volume: Rectification of osmotic flow*. Biochim. Biophys. Acta, *196*:53–65.

Finkelstein, A. (1974) Aqueous pores created in thin lipid membranes by the antibiotics nystatin, amphotericin B and gramicidin A: Implications for pores in plasma membranes. In: Drugs and Transport Processes. B. A. Callingham, ed. University Park Press, Baltimore, pp. 241–250.

Levitt, D.G. (1973) Kinetics of diffusion and convection in 3.2 Å pores. Biophys. J., *13*:186–206.

Macey, R.I. (1979) Transport across single biological membranes. In: Membrane Transport in Biology. G. Giebisch, D.C. Tosteson and H.H. Ussing, eds. Springer-Verlag, Berlin, Vol. 2, pp. 1–57.

Macey, R.I., J.S. Adorante, and F.W. Orme (1978) Erythrocyte membrane potentials determined by hydrogen ion distribution. Biochim. Biophys. Acta, *512*:284–295.

Macey, R.I., D.M. Karan, and R.E.L. Farmer (1972) Properties of water channels in human red cells. In: Biomembranes. F. Kreuzer and J.F.G. Slegers, eds. Plenum Publishing Co., New York, Vol. 3, pp. 331–340.

Owicki, J.C., B.R. Lentz, A.T. Hagler, and H.A. Scheraga (1975) Structure of liquid water. III. Thermodynamic properties of liquid deuterium oxide. J. Phys. Chem., *79*:2352–2361.

Parpart, A.K. (1945) *The permeability of the mammalian* erythrocyte to deuterium oxide (heavy water). J. Cell. Comp. Physiol., *7*:153–162.

Rich, G.T., R.I. Sha'afi, A. Romualdez, and A.K. Solomon (1968) Effect of osmolality on the hydraulic permeability coefficient of red cells. J. Gen. Physiol., *52*:941–954.

Solomon, A.K. (1968) Characterization of biological membranes by equivalent pores. J. Gen. Physiol., *51*:335S–364S.

Thomson, J.F. (1963) Biological Effects of Deuterium. The MacMillan Company, New York.

Trauble, H. (1971) The movement of molecules across lipid membranes: A molecular theory. J. Memb. Biol., *4*:193–208.

Vieira, F.L., R.I. Sha'afi, and A.K. Solomon (1970) The state of water in human and dog red cell membranes. J. Gen. Physiol., *55*:451–466.

FIGURE 9

Effect of Pressure on Osmotic Water Permeability
of Human Red Cells

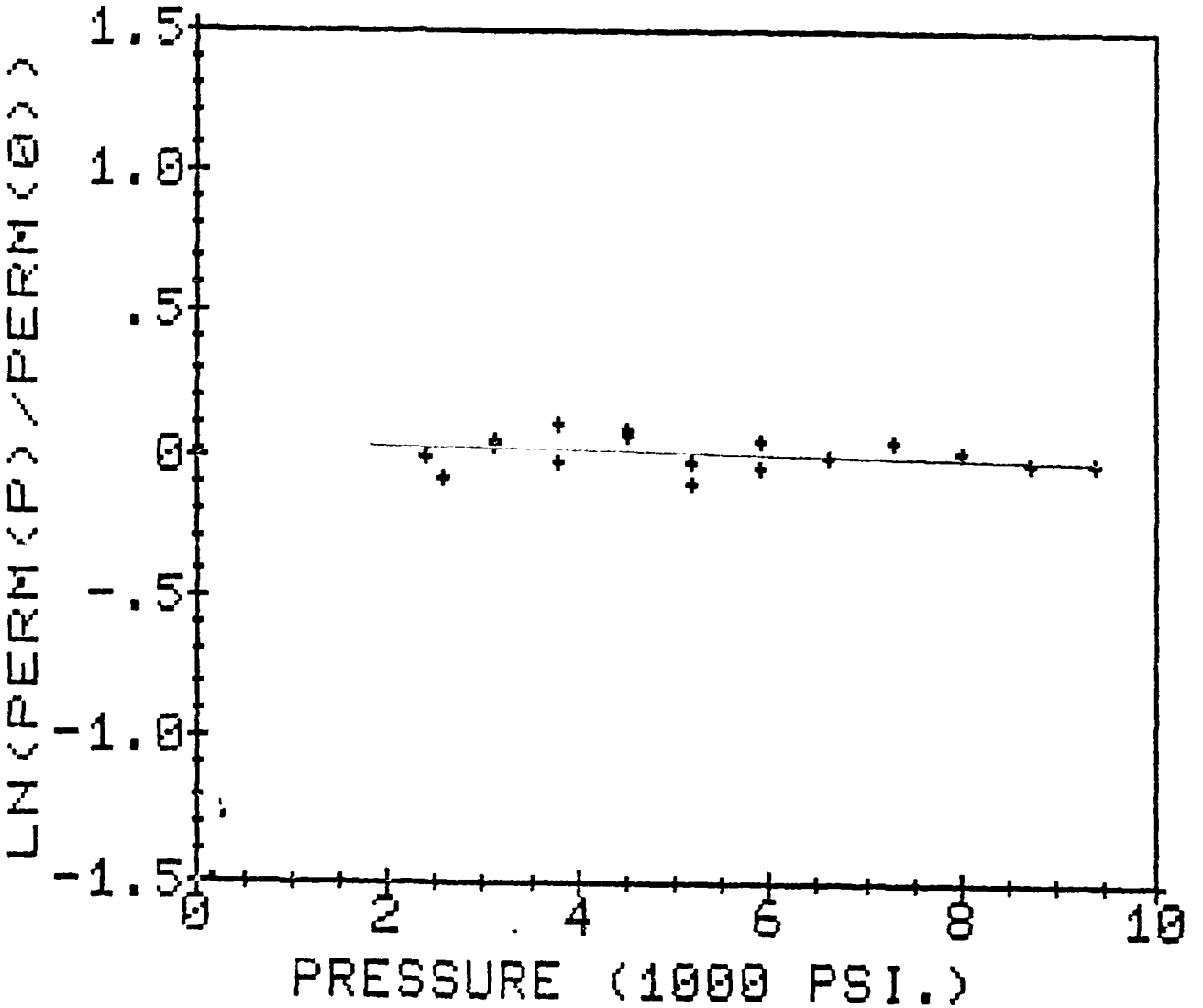

The corresponding activation volume equals 0.71 ml/mole.

REFERENCES

Caswell, A.H. J. Membr. Biol. 7:345-364, 1972.

Cuddeback, , Koeller, R.L. and Dricklamer, H.G. J. Chem. Phys. 21:589, 1953.

Cutter, W.G., McMickle, R.H., Webb, W. and Shiessler, R.W. J. Chem. Physiol. 29:727-740, 1958.

Diamond, J.M. and Wright, E.M. Ann. Rev. Physiol. 31:581-646, 1969.

Drost-Hansen, W. Symp. Soc. Exptl. Biol. 26:61-101, 1972.

Hallett, M., Schneider, A.S. and Carbone, E. J. Membr. Biol. 10:31-44, 1972.

Isaacs, N.S. Liquid Phase High Pressure Chemistry, John Wiley & Sons:New York, 1981.

Johnson, S.M., Miller, K.W. and Bangham, A.D. Biochim. Biophys. Acta 307:42-57, 1973.

Johnson, S.M. and Miller, K.W. Biochim. Biophys. Acta 375:286-291, 1975.

Lew, V.L. and Ferreira, H.G. The effect of Ca on the K permeability of red cells. In: Membrane Transport in Red Cells (ed: J. Clive Ellory and V.L. Lew), Academic Press, New York, 1977. pp. 93-100.

Macey, R.I. Transport of water and nonelectrolytes across red cell membranes. In: Membrane Transport in Biology, Vol. II (ed: G. Giebisch, D.C. Tosteson and H.H. Ussing), Springer-Verlag, New York, 1979. pp. 1-57

Macey, R.I., Karan, D.M. and Farmer, R.L. Properties of water channels in human red cells. In: Biomembranes, Vol. 3 (ed: F. Kreuzer and J.F.G. Slegers), Plenum, New York, 1972. pp. 331-340.

Mikkelson, R.B. and Wallach, D.F.H. Biochim. Biophys. Acta 363:1211-1218, 1974.

Parpart, A. and Green, J.W. J. Cell Comp. Physiol. 38:347-360, 1951.

Podolsky, R.J. J. Physiol. 132:38P-39P, 1956.

Redwood, W.R., Rall, E. and Morales, M. Biochemistry 4:1958-1965, 1965.

Schantz, E.J. and Lauffer, M.A. Biochemistry 4:658, 1962.

Tolberg, A.B. and Macey, R.I. J. Cell Physiol. 79: 43-52, 1972

Trauble, H. J. Membr. Biol. 4:193, 1971.


DATE
ILME